Robust EEG Source Localization Using Subspace Principal Vector Projection Technique

Amita Giri
Electrical Engineering Dept.
Indian Institute of Technology Delhi
New Delhi, India
Amita.Giri@ee.iitd.ac.in

Lalan Kumar
EE & Bharti School of Telecommunication
Indian Institute of Technology Delhi
New Delhi, India
lkumar@ee.iitd.ac.in

Tapan Gandhi
Electrical Engineering Dept.
Indian Institute of Technology Delhi
New Delhi, India
tgandhi@ee.iitd.ac.in

***Abstract*—ElectroEncephaloGram (EEG) signals based Brain Source Localization (BSL) has been an active area of research. The performance of BSL algorithms is severely degraded in the presence of background interferences. Pre-Whitening (PW) based approach to deal with such interference assumes temporal stationarity of the data which does not hold good for EEG based processing. Null Projection (NP) based approach relaxes the temporal stationarity. However, the strict spatial stationarity of the number of interfering sources is maintained between control state and activity state measurement. In practical scenarios where an interference source that exists only in the control state, and does not appear in activity state, NP based approach removes a higher dimension space from the activity data leading to its poor performance. The proposed Subspace Principal Vector Projection (SPVP) based approach utilizes subspace correlation based common interference statistics and thus relaxing the strict spatial stationarity condition. In particular, SPVP based MUltiple SIgnal Classification (MUSIC) and Linearly Constrained Minimum Variance (LCMV) algorithms are presented for BSL. Simulation and experiment with real EEG data from Physionet dataset involving motor imagery task illustrate the effectiveness of the proposed algorithms in robust BSL with interference suppression.**

***Index Terms*—EEG, Source localization, MUSIC, LCMV, Interference suppression, Subspace correlation, Principal vector.**

I. Introduction

Localization of brain cortical activity using high temporal resolution ElectroEncephaloGram (EEG) signals continues to be an active area of research because of its clinical [1]–[3] and research applications [4], [5]. EEG based Brain Source Localization (BSL) involves estimation of electric dipole location and orientation from non-invasive brain potential measurements. The underlying EEG dipole source localization is an ill-posed inverse problem and has an infinite number of possible solutions associated with the measured data. Hence, the unique relationship between the scalp recorded EEG and neural sources may not exist [6]. To solve this inverse problem, a priori assumption is needed to constrain the space of feasible solutions. A priori assumption based on the number of active source dipole is the most classical approach. In particular, underdetermined and overdetermined approach to BSL referred as distributed source model and dipole fitting respectively are utilized. In underdetermined source model, the number of dipoles distributed within the brain volume is considered to be large when compared to the order of the sensor array measurement. On the other hand, the dipole fitting models assume that the electrical activity of the brain can be represented by a small number of Equivalent Current Dipoles (ECD), resulting in an over-determined inverse problem. The widely used dipole fitting methods include MUltiple SIgnal Classification (MUSIC) [7] and Linearly Constrained Minimum Variance (LCMV) [8]. The performance of such methods is limited. It is because the Signal of Interest (SoI) is very weak and buried in spatially correlated noise. The performance is further affected in presence of an interference.

The interference suppression techniques like Pre-Whitening (PW) [9] and Null Projection (NP) [10] methods use a set of 'control state' measurements taken before the stimulus in order to assess the background interference and noise statistics. The control state statistics is utilized to suppress interference effect in the 'activity state' data which is obtained after the stimulus is applied. It is to be noted that some of the interference present in the control state, do not appear in activity state. However, the pre-whitening and null projection based methods try to remove the entire dimension space for interference suppression. This limits the dimensionality of space available for true source estimation and thus affecting the performance of the dipole fitting methods for localization [10]. Subspace Principal Vector Projection (SPVP) based approach is proposed in this paper for efficient interference suppression. Experimental results indicate the robust performance of the proposed algorithms when compared with null projection method.

II. Forward data model

Forward data model in spatio-temporal domain accounts for change in potential w.r.t. space and time. The head volume conductor is modelled by Three Layer Concentric Spherical Head (TLCSH) model [11], in which the brain, skull and scalp are represented using three concentric spheres of homogeneous conductivity. The innermost sphere of radius r_1 is the brain surrounded by skull with concentric shell of radius r_2. This is followed by scalp layer with radius R. The neural tissues in brain and scalp have the same conductivity, denoted by σ. The conductivity of skull is represented by σ_s.

This work was funded by Prime Minister's Research Fellowship (PMRF), Government of India.

A dipole placed on z axis with dipole moment in positive xz plane, is considered in brain region of the three shell model. The EEG potential $V(\theta_k, \phi_k)$ measured at kth sensor location due to a source with unit intensity is given by [12]

$$V(\theta_k,\phi_k) = \left(\frac{1}{4\pi\sigma}\right)\sum_{n=1}^{\infty}\frac{2n+1}{n}b^{n-1}\left[\frac{\xi(2n+1)^2}{d_n(n+1)}\right] \times [n\ o_r P_n(cos(\theta_k)) + o_t P_n^1(cos(\theta_k))cos(\phi_k)], \quad (1)$$

where b is the eccentricity of dipole given as (z/R), and $\xi = \sigma_s/\sigma$. θ is the elevation angle measured downward from positive z axis, and ϕ is the azimuth angle measured anticlockwise from positive x axis. $P_n(cos(\theta_k))$ is Legendre polynomial, $P_n^1(cos(\theta_k)$ is Associated Legendre polynomials (ALPs) and n is the order of the Legendre polynomial. o_r and o_t are the radial and tangential component of the dipole orientation. d_n is expressed as

$$d_n = [(n+1)\xi + n]\left[\frac{n\xi}{n+1}+1\right] + [(n+1)\xi+n] \times (1-\xi)(f_1^{2n+1} - f_2^{2n+1}) - n(1-\xi)^2(\frac{f_1}{f_2})^{2n+1},$$

where $f_1 = r_1/R$, $f_2 = r_2/R$. Potential due to a dipole at any other arbitrary location and orientation, can be obtained by rotating the coordinate system suitably.

The potential at K EEG electrodes due to P active dipoles can now be written in linear separable form as [13]

$$\mathbf{V}_{K\times T} = \mathbf{G}_{K\times 3P}\mathbf{D}_{3P\times T}, \quad (2)$$

where $\mathbf{G}$ is the Gain matrix, $\mathbf{D}$ is the dipole moment matrix and T is number of time snapshots. The detailed expression of each term can be seen in [13] and is not presented herein because of space limitation. Under fixed dipole assumption, the dipole moment matrix can be decomposed as $\mathbf{D}_{3P\times T} = \mathbf{M}_{3P\times P}\mathbf{S}_{P\times T}$, where $\mathbf{M}$ represents unit orientation moments and $\mathbf{S}$ is moment intensity matrix. Substituting this in (2), the final spatio-temporal data model in the presence of spatial and temporal zero mean white Gaussian noise $\mathbf{Z}$ with variance σ^2 can be written as

$$[\mathbf{V}]_{K\times T} = [\mathbf{A}]_{K\times P}[\mathbf{S}]_{P\times T} + [\mathbf{Z}]_{K\times T} \quad (3)$$

where $\mathbf{A}_{K\times P} = \mathbf{G}_{K\times 3P}\mathbf{M}_{3P\times P}$, is the lead field matrix.

III. Source Localization Algorithm

In the MUSIC algorithm, the estimates of active source location are obtained by projecting the Lead Field Vector (LFV) over the estimated noise subspace. Lead field vector $\vec{\mathbf{a}}(\vec{r}_p, \vec{m}_p) \in \mathbf{A}$ is function of location $\vec{r}_p$ and orientation moment $\vec{m}_p \in \mathbf{M}$. Noise subspace $\mathbf{E}_n$ is estimated from the eigen value decomposition of the covariance matrix $\mathbf{R}_v = E[\mathbf{V}\mathbf{V}^T]$. The Cost function of MUSIC spectrum can be written as

$$\mathbf{J}(\vec{r}_p,\vec{m}_p)_{MUSIC} = \frac{\vec{\mathbf{a}}^{\mathbf{T}}(\vec{r}_p,\vec{m}_p)\vec{\mathbf{a}}(\vec{r}_p,\vec{m}_p)}{\vec{\mathbf{a}}^{\mathbf{T}}(\vec{r}_p,\vec{m}_p)\mathbf{E}_n\mathbf{E}_n^T\vec{\mathbf{a}}(\vec{r}_p,\vec{m}_p))}, = \frac{\vec{m}_p^T\mathbf{G}^{\mathbf{T}}(\vec{r}_p)\mathbf{G}(\vec{r}_p)\vec{m}_p}{\vec{m}_p^T\mathbf{G}^{\mathbf{T}}(\vec{r}_p)\mathbf{E}_n\mathbf{E}_n^T\mathbf{G}(\vec{r}_p)\vec{m}_p} \quad (4)$$

For isolated estimation of location and orientation parameters, following generalized eigen value problem [14] is formulated.

$$\mathbf{G}^{\mathbf{T}}(\vec{r}_p)\mathbf{E}_n\mathbf{E}_n^T\mathbf{G}(\vec{r}_p)\vec{m}_p = \lambda\mathbf{G}^{\mathbf{T}}(\vec{r}_p)\mathbf{G}(\vec{r}_p)\vec{m}_p \quad (5)$$

Utilizing, Singular Value Decomposition (SVD) of $\mathbf{G}(\vec{r}_p) = \mathbf{U}_{\mathbf{G}}\mathbf{\Sigma}\mathbf{V}_{\mathbf{G}}^T$, the generalized eigen value problem in (5) can be expressed as

$$\mathbf{U}_{\mathbf{G}}^T\mathbf{E}_n\mathbf{E}_n^T\mathbf{U}_{\mathbf{G}}[\mathbf{\Sigma}\mathbf{V}_{\mathbf{G}}^T\vec{m}_p] = \lambda[\mathbf{\Sigma}\mathbf{V}_{\mathbf{G}}^T\vec{m}_p] \quad (6)$$

Utilizing (5) and (6), the MUSIC spectrum in (4), can now be written as

$$\mathbf{J}(\vec{r}_p,\vec{m}_p)_{MUSIC} = 1/\lambda_{min}(\mathbf{U}_{\mathbf{G}}^T\mathbf{E}_n\mathbf{E}_n^T\mathbf{U}_{\mathbf{G}}) \quad (7)$$

where $\lambda_{min}(.)$ is the minimum eigen value of $(.)$.

The LCMV beamformer attempts to minimize the beamformer output power subject to a unity gain constraint at desired source location. The cost function of LCMV beamforming is given by

$$\mathbf{J}(\vec{r}_p,\vec{m}_p)_{LCMV} = \frac{\vec{\mathbf{a}}^{\mathbf{T}}(\vec{r}_p,\vec{m}_p)\vec{\mathbf{a}}(\vec{r}_p,\vec{m}_p)}{\vec{\mathbf{a}}^{\mathbf{T}}(\vec{r}_p,\vec{m}_p)\mathbf{R}_v{}^{-1}\vec{\mathbf{a}}(\vec{r}_p,\vec{m}_p)} \quad (8)$$

For isolated estimation of source parameters, the cost function of LCMV spectrum can also be formulated in similar fashion expressed as

$$\mathbf{J}(\vec{r}_p,\vec{m}_p)_{LCMV} = 1/\lambda_{min}(\mathbf{U}_{\mathbf{G}}^T\mathbf{R}_v{}^{-1}\mathbf{U}_{\mathbf{G}}) \quad (9)$$

The P highest peaks in MUSIC and LCMV spectrum correspond to active dipole sources. However, the performance of such methods are severely limited by the presence of spatially correlated background noise and interference. In the following section, we briefly describe the existing interference suppression approach and their limitations.

IV. Null Projection Based BSL with Interference Suppression

In this section, the existing NP based approach [15] to BSL with interference suppression is detailed. Pre-whitening approach for interference suppression being simplistic is not considered herein. The data model for control and activity state measurement are represented as

$$\mathbf{Control\ \ State}: \mathbf{V}_C = \mathbf{A}_I\mathbf{S}_{IC} + \mathbf{Z}_C \quad (10)$$

$$\mathbf{Activity\ \ State}: \mathbf{V}_A = \mathbf{A}_S\mathbf{S}_S + \mathbf{A}_I\mathbf{S}_{IA} + \mathbf{Z}_A \quad (11)$$

$\mathbf{V}_C$ is the control state measurement taken prior to the stimulus is applied. It has reliable information about the interference component $\mathbf{A}_I\mathbf{S}_{IC}$ and the spatially white background noise, $\mathbf{Z}_C$. $\mathbf{V}_A$ is the activity state data measured after the stimulus is applied. It consists of signal component $\mathbf{A}_S\mathbf{S}_S$ along with the interference component $\mathbf{A}_I\mathbf{S}_{IA}$, and the background spatially white noise $\mathbf{Z}_A$. Lead field matrix of interference and signal of interest is represented by $\mathbf{A}_I$ and $\mathbf{A}_S$ respectively. $\mathbf{S}_{IC}$ and $\mathbf{S}_{IA}$ is the dipole moment intensity matrix during the control state and activity state. Rows of $\mathbf{S}_{IA}$ will be kept zero for the interfering sources that are present only in the control state and do not appear in the activity state. The number of dipole

source and interference source is represented by N_S and N_I respectively.

Null projection based method nullifies the interference factor of the activity state measurement without pre-whitening it [9]. Thus the NP based method relaxes the temporal stationarity assumption for interferences. However, the spatial stationarity (stationarity w.r.t. number and spatial location of the interferences across control and activity state) assumption still holds. A projection operator orthogonal to the interference is utilized to nullify its influence in the activity data. The projection operator is estimated from control data by solving the following least square problem,

$$\mathbf{N} = \arg\min_{\mathbf{N}} \|\mathbf{N}^T \mathbf{V}_C\|_F^2 \tag{12}$$

subject to the constraint $\mathbf{N}^T\mathbf{N} = \mathbf{I}$. The solution $\mathbf{N}$ comprises of null subspace vectors obtained from singular value decomposition of the control state data. The SVD of the control data is written as

$$\mathbf{V}_C = \begin{bmatrix}\mathbf{U}_{IC} & \mathbf{U}_{ZC}\end{bmatrix} \begin{bmatrix}\Sigma_{IC} & 0 & 0 \\ 0 & \Sigma_{ZC} & 0\end{bmatrix} \begin{bmatrix}\mathbf{W}_{ZC}^T\end{bmatrix} \tag{13}$$

where $\mathbf{U}_{ZC}$ is collection of left singular vectors associated with $K - N_I$ smallest singular values constituting $\mathbf{N} = \mathbf{U}_{ZC}$. The projection matrix $\mathbf{P}_n$, orthogonal to interferences, can now be defined as

$$\mathbf{P}_n = \mathbf{N}\mathbf{N}^T \tag{14}$$

The contribution of interference is removed by projecting the activity state measurements onto the subspace defined by $\mathbf{P}_n$. The null projected data is given by

$$\mathbf{V_{NP}} = \mathbf{P}_n \mathbf{V}_A \tag{15}$$

This alters the lead field vector. The MUSIC and LCMV spectrum can now be computed using new lead field vector given by

$$\vec{\mathbf{a}}_{np}(\vec{r}_p, \vec{m}_p) = \mathbf{P}_n \vec{\mathbf{a}}(\vec{r}_p, \vec{m}_p) \tag{16}$$

NP based source localization algorithms is observed to have accurate interference suppression when compared to pre-whitening based algorithms. NP based approach relaxes the temporal stationarity. However, the strict spatial stationarity w.r.t. number of interferences sources is maintained across control and activity state measurements. In the following Section, relaxing strict spatial stationarity assumption results in efficient interference suppression is investigated.

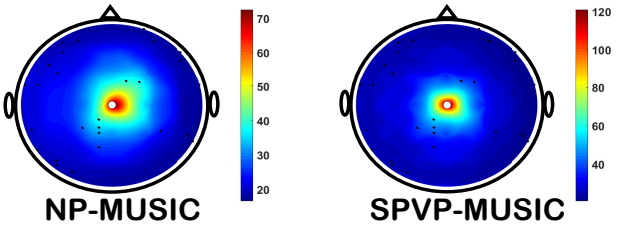

Fig. 1: Spatial spectrum of NP-MUSIC and SPVP-MUSIC.

V. The Proposed SPVP based BSL with Interference Suppression

A performance degradation of NP and PW based methods is observed if spatial stationarity assumption of interference is even partially violated. The number of interference and its location have to be same during control and activity state. In practical scenarios, where a interference source that exists only in the control state and does not appear in activity state, utilization of projection matrix (14), removes a higher dimension space from the activity data. This leads to performance degradation of pre-whitening and NP-based localization. The effect is more visible if the interference is present in the proximity of the target. In this Section, we proposed SPVP based localization that relaxes the strict spatial stationarity w.r.t. number of interference active during control and activity state.

The common interference information between control and activity states is exploited from the SVD of the respective state data. The SVD of $\mathbf{V}_A$ can be expressed as

$$\mathbf{V}_A = \begin{bmatrix}\mathbf{U}_{(S,I)A} & \mathbf{U}_{ZA}\end{bmatrix} \begin{bmatrix}\Sigma_{(S,I)A} & 0 & 0 \\ 0 & \Sigma_{ZA} & 0\end{bmatrix} \begin{bmatrix}\mathbf{W}_{ZA}^T\end{bmatrix} \tag{17}$$

where $\mathbf{U}_{(S,I)A}$ is collection of left singular vectors associated with $N_S + N_I$ largest singular values. The repeated interference statistics is now be exploited using subspace correlation between $\mathbf{U}_{(S,I)A}$ and $\mathbf{U}_{IC}$ as in (13). The steps involved in subspace correlation estimation are as follows [14], [16].

1) Compute the SVD of $\mathbf{U}_{(S,I)A}$ and $\mathbf{U}_{IC}$ as

$$\mathbf{U}_{(S,I)A} = [\mathbf{U}_1 \quad \Sigma_1 \quad \mathbf{V}_1^T], \tag{18}$$

$$\mathbf{U}_{IC} = [\mathbf{U}_2 \quad \Sigma_2 \quad \mathbf{V}_2^T] \tag{19}$$

2) Form $\mathbf{Q} = \mathbf{U}_1^T\mathbf{U}_2$ having SVD as

$$\mathbf{Q} = [\mathbf{U}_Q \quad \Sigma_Q \quad \mathbf{V}_Q^T] \tag{20}$$

3) Form the principal vector set as $\mathbf{X_{P}}_A = \mathbf{U}_1\mathbf{U}_Q$, and $\mathbf{X_{P}}_C = \mathbf{U}_2\mathbf{V_Q}$ corresponding to subspace $\mathbf{U}_{(S,I)A}$ and $\mathbf{U}_{IC}$ respectively.

The N_I ordered singular values $s_1 \geq s_2 \cdots \geq s_{N_I}$ obtained from diagonal of Σ_Q matrix, lie between $[0, 1]$. Geometrically, $s_k = cos\theta_k$ represents principal angle between the principal vectors. Alternatively, s_k is the measure of correlation between the two principal vectors.

The column vectors of $\mathbf{U}_Q$ and $\mathbf{V}_Q$ corresponding to high correlation are utilized to form $\hat{\mathbf{U}}_Q$ and $\hat{\mathbf{V}}_Q$ respectively. A new set of principal vectors of matrices $\mathbf{U}_{IC}$ and $\mathbf{U}_{(S,I)A}$ with high correlation can be written as

$$\hat{\mathbf{X}}_{\mathbf{P}A} = \mathbf{U}_1\hat{\mathbf{U}}_Q, \qquad \hat{\mathbf{X}}_{\mathbf{P}C} = \mathbf{U}_2\hat{\mathbf{V}}_Q \tag{21}$$

The subspace principal vector projection matrix orthogonal to interferences present in control state and activity state can now be constructed using $\hat{\mathbf{X}}_{\mathbf{P}A}$ and $\hat{\mathbf{X}}_{\mathbf{P}C}$ as

$$\mathbf{P_{HA}} = \mathbf{I} - \hat{\mathbf{X}}_{\mathbf{P}A}\hat{\mathbf{X}}_{\mathbf{P}A}^T, \quad \mathbf{P_{HC}} = \mathbf{I} - \hat{\mathbf{X}}_{\mathbf{P}C}\hat{\mathbf{X}}_{\mathbf{P}C}^T \tag{22}$$

Here, $\mathbf{P_{HC}}$ is orthogonal to interferences in control state only and is equivalent to null projection matrix $\mathbf{P}_n$ in (14)

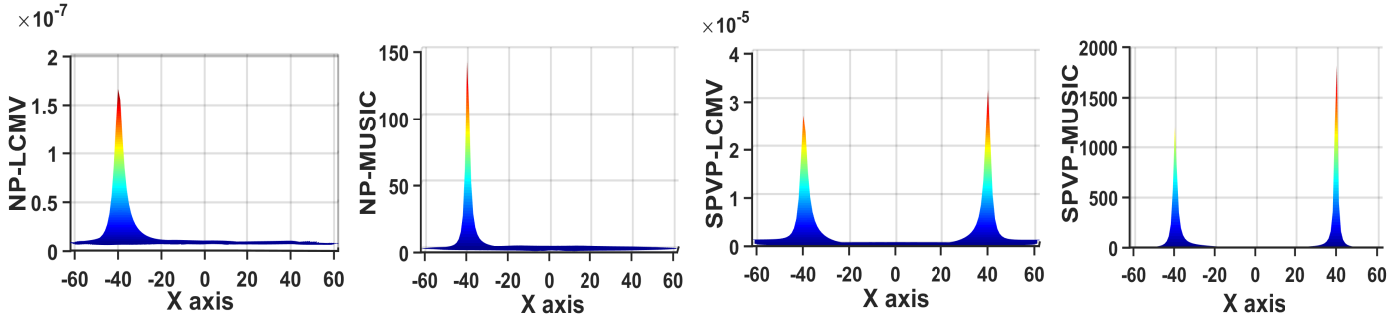

Fig. 2: Cost function plot of NP-LCMV, NP-MUSIC, SPVP-LCMV and SPVP-MUSIC algorithms from left to right respectively.

utilized for final interference suppression. However, this does not take the activity state interferences into account, resulting in poor estimation of target. The projection matrix $\mathbf{P_{HA}}$ considers the correlation of interferences in control and activity state and is orthogonal to interferences common to the two state. Hence, it discreetly nullifies the effect of interference present in the activity state. Thus, the proposed SPVP based approach eliminates the problem of removing higher dimensional subspace from the activity data and improves the target estimation. Rather than $\mathbf{P_{HC}}$, $\mathbf{P_{HA}}$ is utilized to relax the spatial stationarity of interferences. Multiplying (11) by $\mathbf{P_{HA}}$ and utilizing the orthogonality, the data model can be re-written as

$$\mathbf{P_{HA}V}_A = \mathbf{V_{SPVP}} \simeq \mathbf{P_{HA}A}_S\mathbf{S}_S + \mathbf{P_{HA}Z}_A \tag{23}$$

The interference suppressed SPVP potential $\mathbf{V_{SPVP}}$ can now be utilized for localization using MUSIC and LCMV as detailed in Section III, with altered lead field vector as

$$\vec{\mathbf{a}}_{spvp}(\vec{r}_p, \vec{m}_p) = \mathbf{P_{HA}}\vec{\mathbf{a}}(\vec{r}_p, \vec{m}_p) \tag{24}$$

NP and SPVP based MUSIC spectrum is presented in Fig. 1. A single dipole source was placed on the surface of brain near the Cz sensor denoted by white dot. Twenty interferences were placed randomly on the brain surface, represented by black dots. The Signal to Noise Ratio (SNR) and Signal to Interference Ratio (SIR) was set to 10 dB and 5 dB respectively. It may be observed that SPVP based MUSIC has higher spatial resolution when compared to NP counterpart.

VI. Performance Evaluation

Various experiments on brain source localization were conducted to evaluate the performance of the proposed source localization methods in presence of interferenceS. Three layer concentric spherical head model with $R = 10cm$, $f_1 = 0.87$, $f_2 = 0.92$, and $\xi = 0.0125$ [12] was considered for the simulation. The conductivity of scalp, skull and brain was taken to be 0.3360, 0.0042 and 0.3360 S/m respectively. Total 64 sensors were placed over head scalp utilizing 10-20 international electrode placement system. Dipole source location and orientation is assumed to be fixed. Gaussian waveforms with different mean and variance were taken as interference and SoI moment intensity vector. Each signal of interest had unit power. All the interference had the same power. The inter-grid gap was chosen to be 1 mm. Number of snapshot in control and activity state were taken to be 200. Results are presented herein for 100 independent iterations. Effect of control only interference and varying SNR/SIR on BSL is presented using computer simulation. The proposed approach for BSL is additionally verified using real EEG data taken from Physionet dataset involving motor imagery task.

A. Effect of control only interference on BSL

In this section, SPVP based BSL methods are compared with NP counterparts in presence of control only interference. If an interference is present only in the control state and becomes inactive in the activity state, it is referred as control only interference. Two dipole sources of equal power were placed at $\vec{l}_1 = (40, 40, 60)$ mm and $\vec{l}_2 = (-40, 40, 60)$ mm. Four control only interference sources were placed in the neighbourhood of $\vec{l}_1$ at 5mm distance. Additional 16 interfering sources were placed randomly on the brain surface. The SNR and SIR were set to 10 dB and 5 dB respectively. Cost function plot for all the four BSL algorithms is presented in Fig. 2. The source at $\vec{l}_1$ is not localized in NP based approach assuming spatial stationarity and removing the higher dimensional data space. However, SPVP based methods for BSL retain both the sources proving to be robust interference suppression method.

B. Effect of varying SNR and SIR on RMSE

Root Mean Square Error (RMSE) analysis is presented in this section with SNR and SIR varying from -5 dB to 10 dB. A single dipole source was placed on the surface of brain near the Cz sensor and was radially oriented. Twenty interferences were taken for the control and the activity state. RMSE is plotted in Fig. 3 with varying SNR and SIR. It may be noted that SPVP based methods provides better accuracy than the NP counterparts even at the lower SNR and SIR values. Additionally, subspace based MUSIC method outperforms the beamforming based LCMV method.

C. Real data experiment

The proposed SPVP method is also verified using real EEG experimental data corresponding to motor imagery task. Physionet dataset [17] was utilized for this purpose. The data was recorded using 64-channel BCI2000 system during

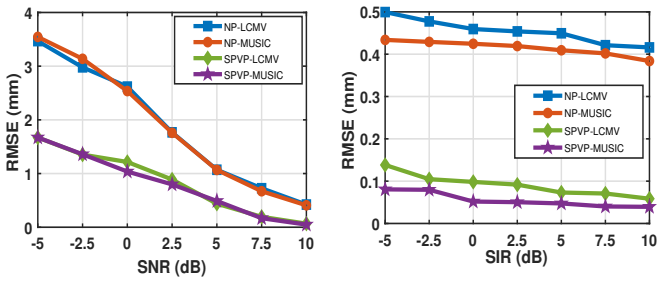

Fig. 3: Effect of varying SNR and SIR on RMSE.

imagery task of opening and closing of left or right hand fist. From the SVD of the control measurement, 95% of the energy was observed to be confined to rank-14 subspace. Hence, the number of interference in the control state was taken to be 14. Spatial spectrum using NP-MUSIC and SPVP-MUSIC method is plotted in Fig. 4. A cortical activation in the contralateral motor area may be seen in both the spectrum as expected. However, SPVP based MUSIC spectrum has pronounced activation in the contralateral motor area only with no additional interference. NP-based localization provides poor localization with additional interferences for such a highly cognitive task.

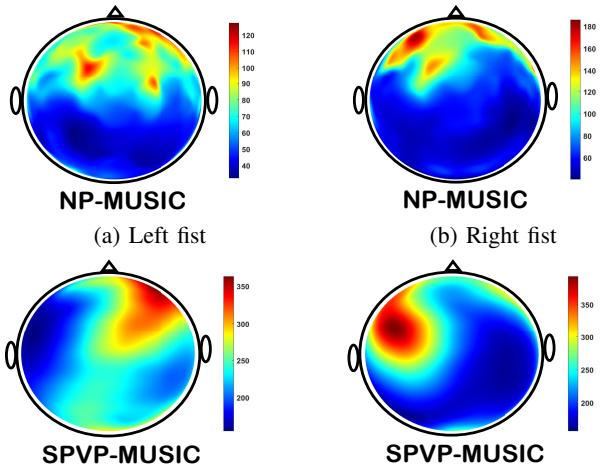

(a) Left fist (b) Right fist

(c) Left fist (d) Right fist

Fig. 4: Spatial spectrum of the NP-MUSIC and SPVP-MUSIC corresponding to motor imagery task.

VII. Conclusion

In this work, Subspace Principal Vector Projection (SPVP) based approach to BSL is presented with efficient interference suppression. In particular, SPVP-MUSIC and SPVP-LCMV methods were formulated. In practical scenarios where an interference source that exists only in the control state, and does not appear in the activity state, NP based approach removes a higher dimension space from the activity data leading to its poor performance. The proposed algorithm utilizes subspace correlation based mutual interference statistics and thus relaxes the strict spatial stationarity condition. Various simulations and experiments with real EEG data show the robustness of the proposed approach. Application of SPVP based BSL with interference suppression is currently being investigated for Brain Computer Interface (BCI) enabled upper limb soft exosuit.

References

[1] C. Plummer, S. J. Vogrin, W. P. Woods, M. A. Murphy, M. J. Cook, and D. T. Liley, "Interictal and ictal source localization for epilepsy surgery using high-density EEG with MEG: a prospective long-term study," *Brain*, vol. 142, no. 4, pp. 932–951, 2019.

[2] E. Tamilia, M. AlHilani, N. Tanaka, M. Tsuboyama, J. M. Peters, P. E. Grant, J. R. Madsen, S. M. Stufflebeam., P. L. Pearl, and C. Papadelis, "Assessing the localization accuracy and clinical utility of electric and magnetic source imaging in children with epilepsy," *Clinical Neurophysiology*, vol. 130, no. 4, pp. 491 – 504, 2019.

[3] A. Giri, L. Kumar, and T. Gandhi, "EEG Dipole Source Localization in Hemispherical Harmonics Domain," in *2018 Asia-Pacific Signal and Information Processing Association Annual Summit and Conference (APSIPA ASC)*. IEEE, 2018, pp. 679–684.

[4] P. Krishnaswamy, G. Obregon-Henao, J. Ahveninen, S. Khan, B. Babadi, J. Iglesias, M. S. Hämäläinen, and P. L. Purdon, "Sparsity enables estimation of both subcortical and cortical activity from MEG and EEG," *Proceedings of the National Academy of Sciences*, 2017.

[5] Y. Huang, L. C. Parra, and S. Haufe, "The New York Head—A precise standardized volume conductor model for EEG source localization and tES targeting," *NeuroImage*, vol. 140, pp. 150 – 162, 2016.

[6] R. Ilmoniemi, M. Hämäläinen, and J. Knuutila, "The forward and inverse problems in the spherical model," *Biomagnetism: Applications and Theory (H. Weinberg, G. Stroink, and T. Katila, eds.), Pergamon Press, New York*, 1985.

[7] J. C. Mosher, P. S. Lewis, and R. M. Leahy, "Multiple dipole modeling and localization from spatio-temporal MEG data," *IEEE Transactions on Biomedical Engineering*, vol. 39, no. 6, pp. 541–557, 1992.

[8] B. D. Van Veen, W. Van Drongelen, M. Yuchtman, and A. Suzuki, "Localization of brain electrical activity via linearly constrained minimum variance spatial filtering," *IEEE Transactions on biomedical engineering*, vol. 44, no. 9, pp. 867–880, 1997.

[9] K. Sekihara, K. E. Hild, S. S. Dalal, and S. S. Nagarajan, "Performance of prewhitening beamforming in MEG dual experimental conditions," *IEEE Transactions on Biomedical Engineering*, vol. 55, no. 3, pp. 1112–1121, 2008.

[10] S. C. Wu, A. L. Swindlehurst, P. T. Wang, and Z. Z. Nenadic, "Projection versus prewhitening for EEG interference suppression," *IEEE transactions on biomedical engineering*, vol. 59, no. 5, pp. 1329–1338, 2012.

[11] S. Rush and D. A. Driscoll, "Current distribution in the brain from surface electrodes," *Anesthesia & Analgesia*, vol. 47, no. 6, pp. 717–723, 1968.

[12] J. P. Ary, S. A. Klein, and D. H. Fender, "Location of sources of evoked scalp potentials: corrections for skull and scalp thicknesses," *IEEE Transactions on Biomedical Engineering*, no. 6, pp. 447–452, 1981.

[13] A. Giri, L. Kumar, and T. Gandhi, "Head Harmonics Based EEG Dipole Source Localization," in *2019 53rd Asilomar Conference on Signals, Systems, and Computers*. IEEE, 2019, pp. 2149–2153.

[14] C. F. Van Loan and G. H. Golub, *Matrix computations*. Johns Hopkins University Press, 1983.

[15] S. C. Wu, A. L. Swindlehurst, and Y. C. Yao, "Direct interference suppression in EEG/MEG dipole source localization," in *2010 IEEE International Conference on Acoustics, Speech and Signal Processing*. IEEE, 2010, pp. 574–577.

[16] J. C. Mosher and R. M. Leahy, "EEG and MEG source localization using recursively applied (RAP) MUSIC," in *Conference Record of The Thirtieth Asilomar Conference on Signals, Systems and Computers*. IEEE, 1996, pp. 1201–1207.

[17] G. Schalk, D. J. McFarland, T. Hinterberger, N. Birbaumer, and J. R. Wolpaw, "BCI2000: a general-purpose brain-computer interface (BCI) system," *IEEE Transactions on biomedical engineering*, vol. 51, no. 6, pp. 1034–1043, 2004.